DSConv: Dynamic Splitting Convolution for Pansharpening

Xuanyu Liu[1*], **Bonan An**[2*]

[1]State Key Laboratory of Photonics and Communications, School of Electronics, Peking University
[2]National Mobile Communications Research Laboratory, Southeast University
xyliu25@stu.pku.edu.cn, bonanan@outlook.com

Abstract

Aiming to obtain a high-resolution image, pansharpening involves the fusion of a multi-spectral image (MS) and a panchromatic image (PAN), the low-level vision task remaining significant and challenging in contemporary research. Most existing approaches rely predominantly on standard convolutions, few making the effort to adaptive convolutions, which are effective owing to the inter-pixel correlations of remote sensing images. In this paper, we propose a novel strategy for dynamically splitting convolution kernels in conjunction with attention, selecting positions of interest, and splitting the original convolution kernel into multiple smaller kernels, named DSConv. The proposed DSConv more effectively extracts features of different positions within the receptive field, enhancing the network's generalization, optimization, and feature representation capabilities. Furthermore, we innovate and enrich concepts of dynamic splitting convolution and provide a novel network architecture for pansharpening capable of achieving the tasks more efficiently, building upon this methodology. Adequate fair experiments illustrate the effectiveness and the state-of-the-art performance attained by DSConv.Comprehensive and rigorous discussions proved the superiority and optimal usage conditions of DSConv.

1 Introduction

Pansharpening aims to compensate for limitations in remote sensing devices, typically constrained by a trade-off between spatial resolution and spectral fidelity, by fusing a low-resolution multispectral image (LR-MSI) and a high-resolution panchromatic image (HR-PANI). With the advancement of remote sensing and communication technologies, pansharpening has become increasingly significant in various domains such as classification [Cao *et al.*, 2020], super-resolution [Du *et al.*, 2013], and detection [Qu *et al.*, 2017]. Recently, pansharpening has made significant improvements because of the superior feature extraction capabilities of convolution neural networks (CNNs), which are mainly based on standard convolutions [Yang *et al.*, 2017; Masi *et al.*, 2016; Deng *et al.*, 2020; Jin *et al.*, 2022a]. A comprehensive review can be found in [Vivone *et al.*, 2020].

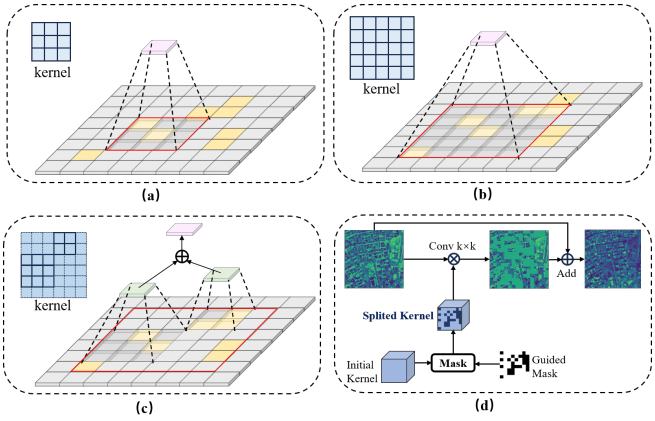

Figure 1: (a) Standard Convolution: Only able to extract local features, making it challenging to capture key features in the input feature map (highlighted in yellow). (b) Large Kernel Convolution: Can capture more crucial information at the cost of increased parameters and computational complexity. (c) DSConv: Proposed method dynamically splits the convolution kernel in the spatial dimension, capturing more key features while improving efficiency. (d) Splitting is achieved by element-wise multiplication of the mask matrix with the convolution kernel, and gradient stability is ensured through residual connections.

The ability to obtain pixel features and optimization is crucial in pansharpening. A smaller receptive field compromises the effect by causing information loss from neighboring pixels, which leads to an urgent need for large kernels [Ding *et al.*, 2022; Peng *et al.*, 2017]. An increasing number of networks are adopting larger kernels to address pansharpening tasks. However, the inevitable escalation in parameter count and computation costs with large kernels has prompted the emergence of numerous optimization methodologies for convolutions. Techniques such as dilated convolutions [Kudo and Aoki, 2017] and depthwise separable convolutions [Sandler *et al.*, 2018] effectively maintain a larger receptive field while substantially reducing the computation overhead, the abilities to extract features are weakened, though. An-

*Equal contribution as first authors.

other methodology from large kernel convolutions involves bolstering the feature extraction capability of input images by applying various convolution kernels [Jin *et al.*, 2022b; Scarpa *et al.*, 2018; Wu *et al.*, 2021a]. Essentially, these approaches harness spatial attention to augment the fitting capacity of convolutions while the spatial invariance is disrupted, rendering them less compatible with computer vision tasks.

The paper proposes a novel approach, dynamic splitting convolution (DSConv), specifically tailored for pansharpening tasks. The proposed method dynamically splits convolution kernels based on the input images, selecting regions of interest for convolution. In this approach, the original convolution kernel is split into multiple smaller kernels, allowing them to adaptively focus on different portions of the input feature, thereby increasing the network's sensitivity to various features. The main contributions are summarized as follows:

1. We propose a novel strategy of convolution kernel splitting, which can split large kernels into several smaller ones with each smaller kernel responsible for processing a local region of the input feature, and we propose a dynamic splitting strategy for feature maps as a further exploration of splitting convolution kernels.

2. A novel strategy of convolution is introduced based on kernel splitting, dynamic splitting convolution (DSConv), which can easily replace any standard convolution in CNNs. Furthermore, we provide the DSC-ResBlock, a novel architecture designed for pansharpening, applying DSConv.

3. Proposed DSConv offers easy optimization, excellent information extraction abilities, and end-to-end training. The effectiveness of the proposed method is validated through theoretical analysis, ablation studies, and fair experiments, whose results demonstrate our model achieves the best performance compared to the state-of-the-art methods.

2 Related Works and Motivation

2.1 Deep Learning Methods for Pansharpening

Convolution neural networks (CNNs) has led to the most effective results in pansharpening tasks, primarily due to their capability to extract high-frequency details from images. PNN [Masi *et al.*, 2016], the first CNN-based pansharpening method, had a simple network structure, resulting in relatively poor performance. PanNet [Yang *et al.*, 2017] segmented the pansharpening task into two objectives: spectral fidelity preservation and spatial detail injection, exhibiting robust generalization abilities but limited spatial detail extraction capabilities. DiCNN [He *et al.*, 2019], with a lower parameter and computation load, featured an overly simple structure that weakened its feature extraction capability. FusionNet [Deng *et al.*, 2021] amalgamated traditional and deep learning approaches, estimating a nonlinear injection model via deep network structures, showcasing strong spectral fidelity and spatial detail representation. However, its complex structure led to extended training times. LAGConv [Jin *et al.*, 2022b] aimed to enhance network performance through adaptive convolution modules and global biases, albeit at the expense of a complex structure and larger parameter count. LGPConv [Zhao *et al.*, 2023] employed learnable Gaussian perturbations to reduce parameters based on channel correlations but exhibited weaker feature extraction capabilities.

2.2 Adaptive Convolution

Adaptive Convolutions dynamically adjust convolution kernels based on input features [Zamora Esquivel *et al.*, 2019; Su *et al.*, 2019], enhancing the flexibility and efficacy of CNNs. But as each pixel has a unique filter, this could lead to increased training time as the network needs to learn more parameters. Involution [Li *et al.*, 2021] proposes spatial specificity and channel invariance, achieving significant advantages in terms of parameter size, computational complexity while causing poor interaction of information between channels. LAGConv [Jin *et al.*, 2022b] generates local-context adaptive convolution kernels and introduces a new global harmonic bias mechanism while increasing computational complexity due to the need for unique filters at each pixel.

Although the methods above have shown significant improvements in multiple visual tasks [Guo *et al.*, 2022], they tend to have fixed and indivisible kernel sizes and generally increase parameter count and computation costs.

2.3 Convolution Kernel Decomposition

Convolution splitting decomposes the original large convolution kernel into multiple small convolution kernels, allowing the network to process input features more flexibly. Inception [Szegedy *et al.*, 2016] performs well in extracting complex features by using convolution kernels of different sizes, but has high computation complexity and faces the problem of gradient disappearance or gradient explosion. Decoupled dynamic filter [Zhou *et al.*, 2021] improves network performance by decoupling deep dynamic filters into spatial and channel dynamic filters, but cannot obtain multi-scale features well. Visual attention network [Guo *et al.*, 2023] decomposes convolution into depth-wise convolution, depth-wise dilation convolution, and point-wise convolution, proposing large kernel attention, but there are still redundant calculations.

The approaches above have been predominantly static in their convolution splitting and haven't explored dynamic splitting under the involvement of attention.

2.4 Motivation

Although various CNN methods exist, there are still some that have not been fully discussed, such as reducing redundant calculations and increasing the receptive field. The advantages of CNNs in extracting high-frequency information have not been fully explored. Remote sensing images possess essential features in terms of pixel correlations and global structure, suggesting the necessity and significance of the explorations.

The diversity and independence of subjects in images, such as buildings and roads, suggest that their information should be separately processed to achieve a better sharpening effect. However, due to the spatial invariance, standard convolutions are unable to perform such an operation, leading to potential distortions at the edges of different subjects in the sharpened image results, which can be explained by the aliasing caused by dense convolution. And in the process of convolution operations, many calculation positions contribute very

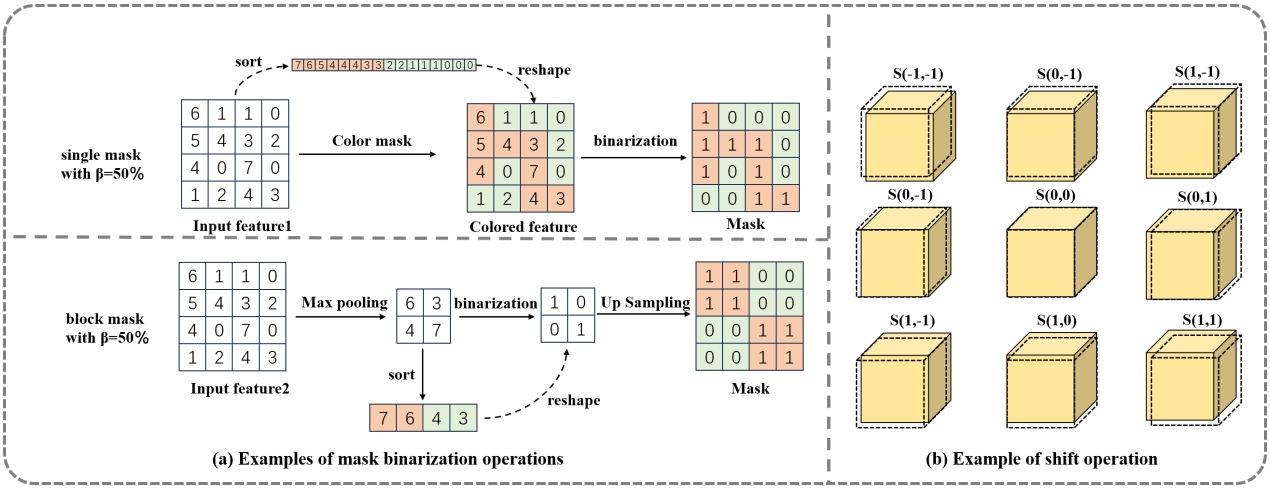

Figure 2: Left section: Examples of mask binarization operations which are 1×1 mask block with $\beta = 50\%$, 2×2 mask block with $\beta = 50\%$. Right section: Examples of mask binarization operations which are 1×1 mask block with $\beta = 0.5$, 2×2 mask block with $\beta = 0.5$, 2×2 mask block with $\beta = 0.25$.Example of $\mathcal{SHIFT}$ operation. The yellow section represents the tensor before the operation, and the dashed box indicates the tensor after the $\mathcal{SHIFT}$.

little, leading to computation redundancy and difficulties in feature extraction.

Masks are applied in deep learning to find regions of interest and apply attention mechanism,s which are common in natural language processing tasks [Vaswani *et al.*, 2017]. Similarly, masks also have great potential in computer vision tasks. Research in self-supervised learning has demonstrated that applying high proportion masking can accelerate training and enhance precision [He *et al.*, 2022]. While there are few explorations of the application of masks in computer vision tasks, no work has attempted to apply masks to splitting convolution kernels previously, which is a good way to improve training efficiency and generalization performance.

Therefore, we propose dynamically splitting convolution kernels, which facilitates the selection of valuable convolution positions through dynamic masking, avoiding information aliasing, reducing redundant computations while improving the network's perceptual capability for input information. Moreover, this method accelerates convolutions through controllable parameter splitting and performs exceptionally well in accomplishing pansharpening tasks when combined with adaptive convolution.

Different from existing sharpening methods, the proposed DSConv applies the splitting operation to convolution kernels and selectively splits them based on the features of the input data, reducing redundant computations, which contributes to improved computation efficiency, especially when dealing with large-scale data. DSConv can dynamically choose the splitting mode and position, allowing the network to be more flexible and efficient when handling pansharpening tasks.

3 Methodology

In this section, we will demonstrate the details of DSConv, mainly focusing on the splitting operation of convolution kernels and the selection method of masks for feature extraction.

3.1 Dynamic Convolution Splitting

To begin with, we provide a concise overview of the standard convolution process. The convolution kernel undergoes a pixel-wise multiplication with the corresponding pixels $I_{i,j} \in \mathbb{R}^{1\times1\times C_{in}}$ of the input feature map, followed by summation to derive the value of the output pixel. This operation involves the movement of the convolution kernel from left to right and top to bottom, employing the defined stride, to generate the pixel values at various locations within the output image, as illustrated in the formula below:

$$Y_{i,j,m} = \sum_{n} \sum_{(u,v)\in\Delta L} K_{m,n,u+[K/2],v+[K/2]} X_{i+u,j+u,n} \tag{1}$$

Where $Y_{i,j,k}$ represents the pixel value at position (i, j) on channel k of the output feature, $X_{i,j,k}$ signifies the pixel value at position (i, j) on channel k of the input feature, and K denotes the standard convolution kernel.

For the sake of simplicity, we define the convolution symbol as $\otimes$. Thus, the convolution operation can be denoted as follows:

$$Y = X \otimes K \tag{2}$$

Where $X \in \mathbb{R}^{C_{in}\times H\times W}$, $K \in \mathbb{R}^{C_{out}\times C_{in}\times K\times K}$, the resulting feature map $Y \in \mathbb{R}^{C_{out}\times H^{'}\times W'}$.

If we involve a subset of the convolution kernel in the convolution process, it can be represented as:

$$Y^{(i)} = X \otimes K^{(i)} \tag{3}$$

where $K^{(i)} \in \mathbb{R}^{C_{out}\times C_{in}\times k\times k}$.

For ease of explanation, we assume that the extracted portion of the convolution kernel is of size 1×1, thus $K^{(i)} \in \mathbb{R}^{C_{\text{out}}\times C_{\text{in}}\times1\times1}$ represents the smaller convolution kernel and

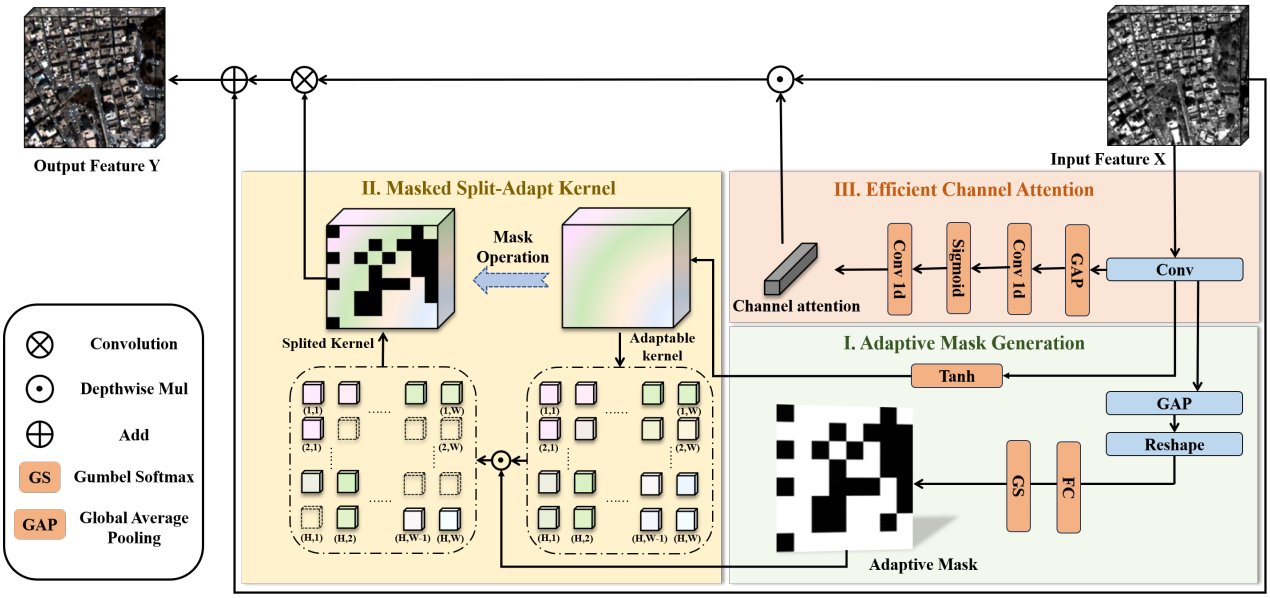

Figure 3: The overview of DSConv architecture. DSConv can be divided into three main parts: Part I (green section) learns the mask matrix. Part II (yellow section) guides the spatial splitting of the convolution kernel using the mask. Part III (orange section) involves channel attention injection. For clarity in presentation, the convolution operations are represented as "Conv", deformation operations as "Reshape", full connected layer as "FC" and activation layers as "RELU" in the flowchart.

$Y^{(i)} \in \mathbb{R}^{C_{\text{out}} \times H' \times W'}$ corresponds to the feature map resulting from the convolution output of this small kernel. Simultaneously, we define $s^{(i)}$, a two-dimensional vector, for $K^{(i)}$ concerning the original large convolution kernel K. This vector $s^{(i)}$ signifies the offset of $K^{(i)}$ relative to the center of the convolution kernel K. For instance, if the selected $K^{(i)}$ precisely aligns with the center of K, then $s^{(i)} = (0, 0)$. If the chosen $K^{(i)}$ aligns with the top right corner of K, then $s^{(i)} = (\frac{K-1}{2}, \frac{K-1}{2})$. For simplicity, we define the $\mathcal{SHIFT}$ operation $\tilde{f} \triangleq \mathcal{SHIFT}(f, s^{(n)})$ [Pan *et al.*, 2022] as

$$\tilde{f}_{i,j} = f_{i+s^{(n)}_{(1)}, j+s^{(n)}_{(2)}}, \forall i, j \tag{4}$$

Thus, the formula for splitting convolution is

$$Y = \sum_{i} \mathcal{SHIFT}(Y, s^{(i)}) \tag{5}$$

The dynamic splitting we proposed utilizes a set $\mathbb{S} = \{s^{(0)}, s^{(1)}, \cdots, s^{(\alpha)}\}$ to denote the valuable positions of the weights on the convolution kernel. $\mathbb{S}$ can be readily transformed into a matrix form, known as the mask matrix:

$$M_{i,j} = \begin{cases} 1, & (i,j) \in \mathbb{S} \\ 0, & (i,j) \notin \mathbb{S} \end{cases} \tag{6}$$

Subsequently, by utilizing the mask to eliminate the weights at positions that hold less value for feature extraction, we obtain elaborately processed irregular small convolution kernels. Employing the concept of splitting convolution, we break down the original convolution kernel. The convolution formula at this stage becomes

$$Y = \sum_{s \in s^{(i)}} \mathcal{SHIFT}(Y, s^{(i)}) \tag{7}$$

In summary, the integration of splitting convolution and mask matrices can effectively reduce redundant weights within the convolution kernels, thereby achieving a more efficient and flexible convolution operation. The following sections will delve into the detailed explanation of the proposed method for generating the adaptive mask matrix, aiming to better facilitate dynamic splitting convolution.

3.2 Adaptive Mask Matrix

The mask serves as a crucial guide to splitting convolution kernels, allowing the original kernels to be dynamically split based on the content of the input data. Further, we integrated the attention mechanism in the generation process of the mask to enhance the feature extraction ability and flexibility. The input image is compressed to a size equivalent to that of the convolution kernel by max-pooling initially, which substantially reduces the resource consumption. Following the principle of data dependency, a single-channel tensor $P \in \mathbb{R}^{1*k*k}$ is obtained through convolution operations.

$$P = X_{pooling} \otimes K' \tag{8}$$

Binaryizing the tensor P to derive the mask M is an important step in which process we strike a balance between computation cost and operational simplicity by adopting the threshold truncation method. Considering factors such as varying image qualities in different tasks and diverse application scenarios, we introduce a hyperparameter β to control the selection of the threshold for truncating tensor P.

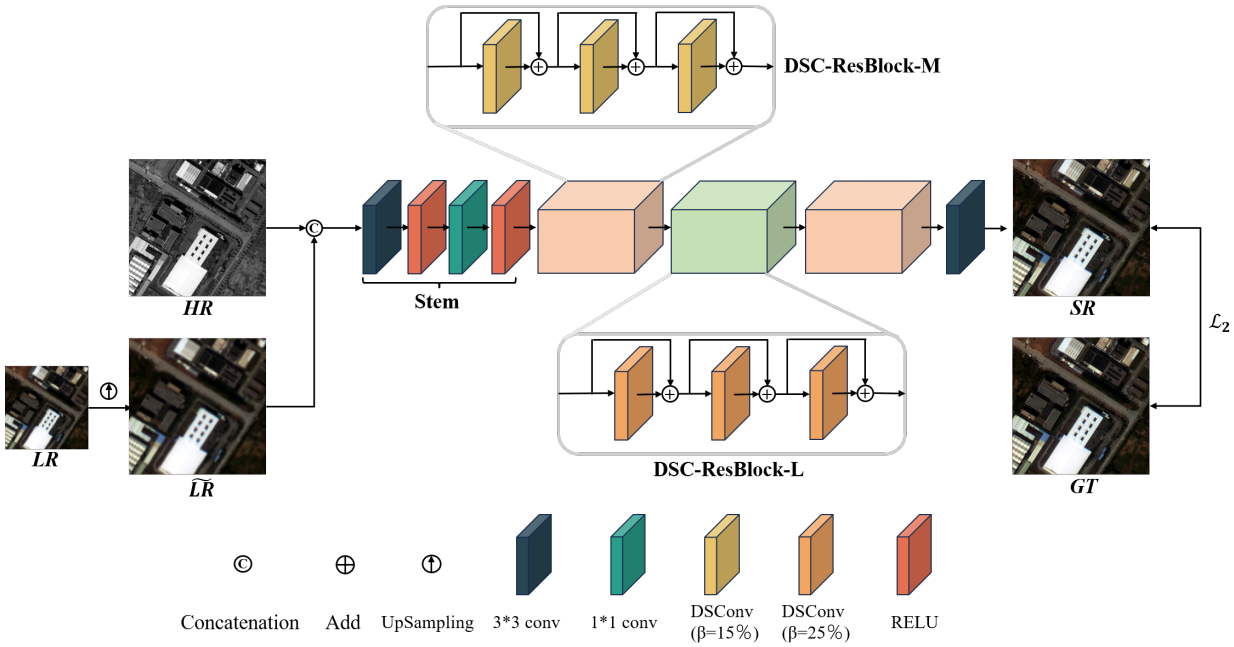

Figure 4: The overall architecture of the proposed DSC-ResNet for pansharpening. The network is composed of a Stem, two DSC-ResBlocks with moderately masked proportions, and one DSC-ResBlock with a highly masked proportion. The blocks with lower masking proportions are designed to extract more semantic information, while the intermediate blocks with higher masking proportions are utilized to filter critical regions.

Given that binarizing to a lower bit depth is sufficient to guide the decomposition of the convolution without incurring a significant amount of additional computation, the method to obtain the mask matrix M is as follows:

$$M_{i,j} = \begin{cases} 1, & P_{i,j} \leq Sort(P, \beta) \\ 0, & P_{i,j} > Sort(P, \beta) \end{cases} \tag{9}$$

The function $Sort(P, \beta)$ returns the minimum value among the smallest $\beta \times 100\%$ elements in matrix P. Generally, β is often set to 20% for optimal performance, which will be fully discussed and explained in the experimental section later on. The specific choice still needs to be adjusted according to the actual task, however. Typically, when the features in the input images are prominent and clear, a lower β is expected to be selected. On the contrary, if the quality of the input images is not satisfactory, features not being distinct, it is advisable to set β higher to filter out interference information.

3.3 Adaptive Dynamic Convolution Splitting

We have extended the dynamic splitting mechanism, which is based on standard convolution, to adaptive convolution to exhibit better adaptability, accommodating changes in inputs more effectively. The mask is extended to be as large as the feature map, selecting regions processed by the adaptive convolution kernels. Simultaneously, we have established a connection between the input features and output features, forming a residual structure, which prevents the preservation of the basic structure in cases where the fitting performance is suboptimal, thereby avoiding the disruption of features. The convolution formula at this stage can be expressed as:

$$Y = \sum_{s^{(i)} \in \mathbb{S}} \mathcal{SHIFT}(X^{(i)} \otimes K^{(i)}, s^{(i)}) + X \tag{10}$$

Where $X^{(i)}$ and $K^{(i)}$ respectively represent the input pixel $X^{(i)} \in \mathbb{R}^{C_{\text{in}} \times 1 \times 1}$ with an offset $s^{(i)}$ relative to the center of the feature map and the corresponding adaptive convolution kernel $K^{(i)} \in \mathbb{R}^{C_{\text{out}} \times C_{\text{in}} \times k \times k}$. Here, S denotes the set of offsets for the selected region indicated by the mask.

3.4 Dynamic Splitting Network Structure

We propose DSC-ResBlock based on dynamic splitting convolution for DSConv can easily replace the standard convolution in any CNN architecture, as shown in Figure 4. We denote the low-resolution multispectral image as "$\mathbf{LR}$", high-resolution panchromatic image as "$\mathbf{HR}$" and the upsampled "$\mathbf{LR}$" as "$\widetilde{\mathbf{LR}}$". The ultimate output, sharpened imag,e is denoted as "$\mathbf{SR}$". The goal of pansharpening is to fuse $\mathbf{LR}$ and $\mathbf{HR}$ to obtain $\mathbf{SR}$.

DSC-ResBlock replaces standard convolutions as DSConvs in the original ResBlock. As shown in Figure 4, the network consists of three parts. After obtaining $\widetilde{\mathbf{LR}}$ by upsampling $\mathbf{LR}$, we concatenate the $\mathbf{HR}$ and $\widetilde{\mathbf{LR}}$ along the channel dimension, which is the input of the network for feature extraction. The first part contains standard convolutions and $\mathbf{ReLU}$ activation layers. Following is DSC-ResBlocks with different masking proportions, blocks masking less extracting features exactly, while that masking

Table 1: Average results on 20 reduced resolution WV3 data and 20 full resolution WV3 images, respectively. (Bold: best)

Method	(a) Reduced resolution WV3 dataset			(b) Full resolution WV3 dataset		
	Q8 ↑	**SAM** ↓	**ERGAS** ↓	D_λ ↓	D_s ↓	**HQNR** ↑
BT-H	0.8324±0.0942	4.9198±1.4252	4.5789±1.4955	0.0574±0.0232	0.0810±0.0374	0.8670±0.0540
BDSD-PC	0.8294±0.0968	5.4293±1.8230	4.6976±1.6173	0.0625±0.0235	0.0730±0.0356	0.8698±0.0531
MTF-GLP-FS	0.8333±0.0923	5.3162±1.7663	4.7004±1.5966	0.0206±0.0082	0.0630±0.0284	0.9180±0.0346
MTF-GLP-HPM-R	0.8346±0.0917	5.3383±1.7632	5.2301±3.0160	0.0197±0.0078	0.0630±0.0289	0.9187±0.0347
TV	0.7952±0.1198	5.6923±1.8078	4.8555±1.4342	0.0234±0.0061	0.0393±0.0227	0.9383±0.0269
PNN	0.8797±0.1021	3.6054±0.9015	2.7756±0.6863	0.0213±0.0080	0.0428±0.0147	0.9369±0.0212
PanNet	0.8763±0.1050	3.5505±0.8837	2.7813±0.7580	0.0165±0.0074	0.0470±0.0213	0.9374±0.0271
DiCNN	0.8864±0.1000	3.5170±0.9047	2.7795±0.7192	0.0362±0.0111	0.0462±0.0175	0.9195±0.0258
MSDCNN	0.8763±0.1009	3.7071±0.9320	2.8755±0.7549	0.0230±0.0091	0.0467±0.0199	0.9316±0.0271
BDPN	0.8573±0.1099	4.1178±1.0214	3.1534±0.7673	0.0364±0.0142	0.0459±0.0192	0.9196±0.0308
FusionNet	0.8906±0.1020	3.2560±0.8266	2.5712±0.6984	0.0239±0.0090	0.0364±0.0137	0.9406±0.0197
LAGConv	0.8961±0.1025	3.0414±0.6901	2.3700±0.6306	0.0368±0.0148	0.0418±0.0152	0.9230±0.0247
DSConv	**0.9091±0.0837**	**3.0154±0.5831**	**2.2547±0.5748**	**0.0133±0.0089**	**0.0325±0.0111**	**0.9459±0.0153**

more selecting the most important positions. The last part is a standard convolution layer to obtain $\mathbf{SR}$.

Therefore, the forward propagation of the network can be represented as:

$$SR = F_\theta(lms, pan) \tag{11}$$

Where F_θ represents a non-linear function with parameters θ. The parameters are continually updated during the gradient back propagation process to make $\mathbf{SR}$ approach the target image GT infinitely. The loss function we designed is as follows:

$$L(\Theta) = \frac{1}{N}\sum_{i=1}^{N} \|F_\theta(lms^{(i)}, pan^{(i)}) - GT^{(i)}\|^2 \tag{12}$$

where N represents the number of training samples, $||\cdot||^2$ denotes the Frobenius norm.

4 Experiments

4.1 Datasets and Training Details

To assess the effectiveness of our method, we conducted fair experiments on the PanCollection dataset [Xiao Wu and Ran, 2022; **?**; Wu *et al.*, 2021b], which comprises diverse satellite data encompassing different spectral bands, resolutions, locations, and surface content. The PanCollection dataset incorporates data from three satellite sensors: an 8-channel WorldView-3 $(WV3)$ dataset, a 4-channel QuickBird (QB) dataset, and a GaoFen-2 $(GF2)$ dataset. The dataset is available for fair use and download.

The $WV3$, QB, and $GF2$ dataset consist of 10,794 $64 \times 64 \times 8$ remote sensing images, 19,044 $64 \times 64 \times 4$ remote sensing images, and 22,010 $64 \times 64 \times 4$ remote sensing images respectively (90% allocated for training, 10% for validation). The test set comprises 20 remote sensing images with a PAN size of 256×256.

We employed the quantitative evaluation metrics discussed in the review for assessing the simulated dataset. The evaluation metrics include SAM (spectral angle mapper), $ERGAS$ (relative dimensionless global error in synthesis), and $Q2n$ (the multi-band extension of the universal image quality index).

Our model was implemented using PyTorch [Paszke *et al.*, 2019] and trained on an NVIDIA 3090. Adam optimizer [Kingma and Ba, 2014] is used to train the model for 500 iterations with fixed hyperparameters $\beta_1 = 0.9$ and $\beta_2 = 0.999$. Details regarding the model's parameter settings will be discussed in the subsequent sections.

4.2 Comparison with State-of-the-Art

We conducted training and testing using the proposed model and compared it with state-of-the-art methods.

Testing on the 8-channel Simulated Dataset

Table 1 illustrates the results of our proposed method, compared with state-of-the-art approaches on the WV3 dataset. Under similar conditions using the same dataset and training metrics, it is evident that our proposed method outperforms all existing methods. Our method demonstrates remarkable effectiveness ,particularly in ·. Figure X shows the results achieved through various methods. To facilitate clearer observation, we also present error maps. It's evident that our proposed method exhibits the least deviation from the Ground Truth (GT).

Testing on the 4-channel Simulated Dataset

To further emphasize the effectiveness and broad applicability of the proposed approach, experiments were conducted on the QB and GF2 datasets. Table X illustrates the comparative experimental results, where, similarly, the proposed approach achieved superior results.

4.3 Discussion

Ablation Study

To validate the effectiveness of dynamic mask-based convolution splitting, we conducted extensive ablation experiments on the WV3 dataset, which involved: 1) Standard convolution, 2) Dynamic convolution splitting only, 3) Adaptive convolution only, and 4) Employing adaptive dynamic split con-

Table 2: Average results on 20 GF and 20 QB examples, respectively. (Bold: best)

Method	(a) Reduced resolution QB dataset			(b) Reduced resolution GF2 dataset		
	Q4 ↑	SAM ↓	ERGAS ↓	Q4 ↑	SAM ↓	ERGAS ↓
BT-H	0.8326±0.0880	7.1943±1.5523	7.4008±0.8378	0.9177±0.0253	1.6488±0.3603	1.5280±0.4093
BDSD-PC	0.8308±0.0902	8.2606±2.0582	7.5679±0.8240	0.8931±0.0346	1.6763±0.3549	1.6505±0.4371
MTF-GLP-FS	0.8352±0.0895	8.1012±1.9574	7.4098±0.7499	0.8955±0.0350	1.6578±0.3859	1.5994±0.3989
MTF-GLP-HPM-R	0.8403±0.1015	8.0466±1.8942	9.1991±5.7432	0.8985±0.0342	1.6526±0.3934	1.5986±0.4097
TV	0.8214±0.0831	7.5113±1.6636	7.6906±0.9116	0.9071±0.0287	1.9106±0.4468	1.7371±0.4465
PNN	0.9158±0.0975	5.2135±0.9343	4.5004±0.3602	0.9592±0.0098	1.0491±0.2196	1.0592±0.2270
PanNet	0.8830±0.0952	5.8013±1.1600	5.9076±0.8519	0.9660±0.0101	0.9984±0.2064	0.9223±0.1854
DiCNN	0.9011±0.0991	5.3862±0.9999	5.1764±0.4438	0.9582±0.0099	1.0536±0.2237	1.0821±0.2442
MSDCNN	0.9188±0.0966	5.1471±0.9342	4.3828±0.3400	0.9601±0.0106	1.0477±0.2139	1.0423±0.2217
BDPN	0.9005±0.0923	6.1225±1.2106	5.2756±0.6870	0.9242±0.0217	1.4642±0.3133	1.5224±0.4118
FusionNet	0.9231±0.0943	4.9279±0.8878	4.1754±0.3017	0.9628±0.0095	0.9742±0.2051	0.9892±0.2138
LAGConv	0.9314±0.0917	4.5548±0.8155	3.8436±0.4032	0.9796±0.0093	0.7888±0.1436	0.6916±0.1102
DSConv	**0.9342±0.0898**	**4.1806±0.7728**	**3.5752±0.3340**	**0.9807±0.006**	**0.7828±0.1416**	**0.6776±0.1270**

volution kernels. Table 3 presents the results of these ablation experiments. It is apparent that the adaptive split convolution kernels exhibit the best performance. The comparison among dynamic convolution splitting, adaptive convolution, and standard convolution underscores the effectiveness of each component.

Table 3: Test results of ablation experiments for adaptation and the splitting operation. (Bold: best)

adaptation	splitting	Q8 ↑	SAM ↓	ERGAS ↓
✗	✗	0.8895±0.0875	3.6751±0.5125	2.6448±0.6453
✓	✗	0.8945±0.0951	3.4662±0.5832	2.5224±0.6245
✗	✓	0.8985±0.0842	3.4028±0.5382	2.5244±0.5812
✓	✓	**0.9024±0.0751**	**3.3559±0.5021**	**2.4519±0.5368**

Masking Proportions

The hyperparameter β of the mask matrix influences the masking proportion. β with a higher value leads to fewer kernels being split out, while more important positions are selected; conversely, β with a lower value extracts more features. Therefore β has the optimal value for different tasks.

Experiments were conducted on the WV3 dataset to explore the best value of β for pansharpening. Experiment results, as depicted in Table 4, indicate that choosing 20% for β achieves the best performance.

Table 4: Impact of masking proportion on model performance. (Bold: best)

Proportion	Q8 ↑	SAM ↓	ERGAS ↓
10%	0.9022±0.0891	3.2487 ±0.5648	2.3769 ±0.6051
20%	**0.9056±0.0863**	**3.1873 ±0.5849**	**2.3501 ±0.5551**
30%	0.9038±0.0898	3.2245±0.5612	2.3591±0.5795
50%	0.8784 ±0.0977	4.4956 ±0.5887	2.9792 ±0.5741
80%	0.8960 ±0.0933	3.4620 ±0.6531	2.5575 ±0.6872

Comparison With Popular Convolution Methods And Networks

To further demonstrate the effectiveness of the convolution splitting strategy and DSConv, we compare pansharpening results using DSConv with those using large kernel convolution, adaptive convolution, and dilated convolution, respectively. Besides, we replace standard convolutions in PanNet, DiCNN, and FusionNet with DSConv to discuss the superiority of DSConv. As shown in Table 5 and Table 6, our proposed methods achieve the best results.

Table 5: Comparison of Plain Convolution (**Conv.**) and DSConv on three network backbones. (Bold: best)

Networks	SAM ↑		ERGAS ↓		Q8 ↓	
	Conv.	DSConv	Conv.	DSConv	Conv.	DSConv
PanNet	0.89±0.09	**0.90±0.08**	3.72±0.62	**3.21±0.58**	2.66±0.60	**2.41±0.55**
DiCNN	0.89±0.09	**0.90±0.08**	3.68±0.64	**3.18±0.59**	2.63±0.61	**2.38±0.57**
FusionNet	0.90±0.09	**0.91±0.08**	3.66±0.63	**3.15±0.57**	2.65±0.61	**2.40±0.56**

Table 6: Comparison between DSConv and several popular convolution variants. (Bold: best)

Methods	SAM ↑	ERGAS ↓	Q8 ↓
Large Kernel Conv. (k=31)	0.8914±0.089	3.8054±0.679	2.7325±0.620
Large Kernel Conv. (k=9)	0.8941±0.090	3.5976±0.643	2.6265±0.610
Atrous Conv. (dilate=2)	0.8904±0.090	3.6016±0.612	2.6245±0.607
Atrous Conv. (dilate=3)	0.8996±0.089	3.4401±0.641	2.5219±0.634
Atrous Conv. (dilate=4)	0.8963±0.087	3.5431±0.652	2.6020±0.611
Involution	0.9052±0.091	3.2536±0.678	2.3892±0.567
LAGConv	0.9012±0.094	3.2927±0.588	2.4002±0.558
DSConv	**0.9095±0.080**	**3.1458±0.570**	**2.3581±0.562**

5 Conclusions

In this paper, we propose a novel dynamic splitting convolution, DSConv, which selectively splits convolution kernels based on the features, allowing better adaptation to diverse features. Besides, DSConv dynamically chooses the splitting position, enhancing feature representation and fitting capability, contributing to improved computation efficiency and

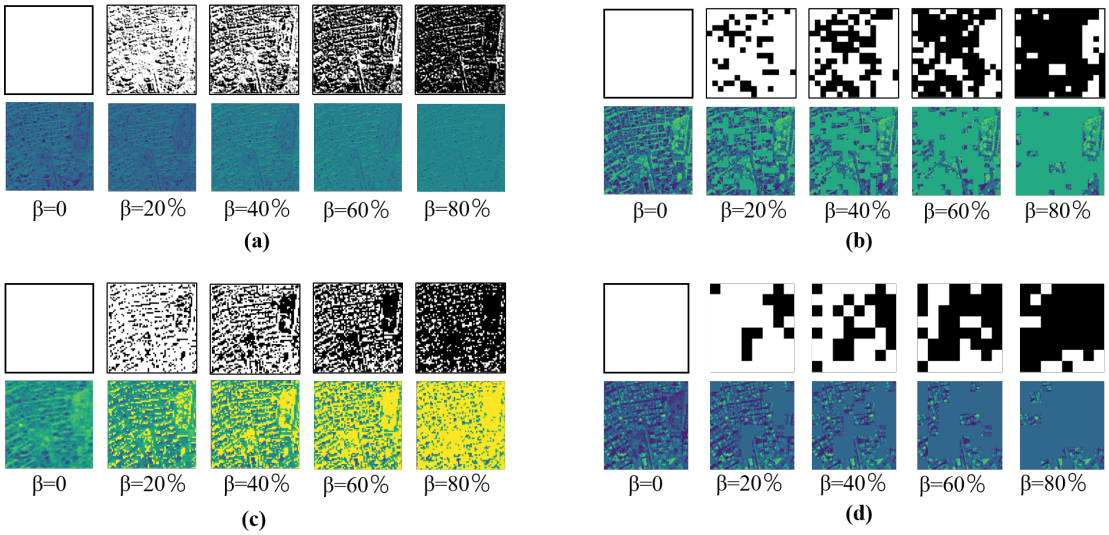

Figure 5: (a) When the resolution is 1×1, the masks and masked features corresponding to different β; (b) When the resolution is 4×4, the masks and masked features corresponding to different β; (c) When the resolution is 2×2, the masks and masked features corresponding to different β; (d) When the resolution is 8×8, the masks and masked features corresponding to different β.

optimization. We further propose the DSC-ResBloc, which applies DSConv to residual blocks for pansharpening tasks. Experiments demonstrated that the proposed method achieves the best results compared with state-of-the-art approaches, and discussions prove the effectiveness and superiority of DSConv.

References

[Cao *et al.*, 2020] Xiangyong Cao, Jing Yao, Zongben Xu, and Deyu Meng. Hyperspectral image classification with convolutional neural network and active learning. *IEEE Transactions on Geoscience and Remote Sensing*, 58(7):4604–4616, 2020.

[Deng *et al.*, 2020] Liang-Jian Deng, Gemine Vivone, Cheng Jin, and Jocelyn Chanussot. Detail injection-based deep convolutional neural networks for pansharpening. *IEEE Transactions on Geoscience and Remote Sensing*, 59(8):6995–7010, 2020.

[Deng *et al.*, 2021] Liang-Jian Deng, Gemine Vivone, Cheng Jin, and Jocelyn Chanussot. Detail injection-based deep convolutional neural networks for pansharpening. *IEEE Transactions on Geoscience and Remote Sensing*, 59(8):6995–7010, 2021.

[Ding *et al.*, 2022] Xiaohan Ding, Xiangyu Zhang, Jungong Han, and Guiguang Ding. Scaling up your kernels to 31x31: Revisiting large kernel design in cnns. In *Proceedings of the IEEE/CVF conference on computer vision and pattern recognition*, pages 11963–11975, 2022.

[Du *et al.*, 2013] Peijun Du, Sicong Liu, Junshi Xia, and Yindi Zhao. Information fusion techniques for change detection from multi-temporal remote sensing images. *Information Fusion*, 14(1):19–27, 2013.

[Guo *et al.*, 2022] Meng-Hao Guo, Tian-Xing Xu, Jiang-Jiang Liu, Zheng-Ning Liu, Peng-Tao Jiang, Tai-Jiang Mu, Song-Hai Zhang, Ralph R Martin, Ming-Ming Cheng, and Shi-Min Hu. Attention mechanisms in computer vision: A survey. *Computational visual media*, 8(3):331–368, 2022.

[Guo *et al.*, 2023] Meng-Hao Guo, Cheng-Ze Lu, Zheng-Ning Liu, Ming-Ming Cheng, and Shi-Min Hu. Visual attention network. *Computational Visual Media*, 9(4):733–752, 2023.

[He *et al.*, 2019] Lin He, Yizhou Rao, Jun Li, Jocelyn Chanussot, Antonio Plaza, Jiawei Zhu, and Bo Li. Pansharpening via detail injection based convolutional neural networks. *IEEE Journal of Selected Topics in Applied Earth Observations and Remote Sensing*, 12(4):1188–1204, 2019.

[He *et al.*, 2022] Kaiming He, Xinlei Chen, Saining Xie, Yanghao Li, Piotr Dollár, and Ross Girshick. Masked autoencoders are scalable vision learners. In *Proceedings of the IEEE/CVF conference on computer vision and pattern recognition*, pages 16000–16009, 2022.

[Jin *et al.*, 2022a] Cheng Jin, Liang-Jian Deng, Ting-Zhu Huang, and Gemine Vivone. Laplacian pyramid networks: A new approach for multispectral pansharpening. *Information Fusion*, 78:158–170, 2022.

[Jin *et al.*, 2022b] Zi-Rong Jin, Tian-Jing Zhang, Tai-Xiang Jiang, Gemine Vivone, and Liang-Jian Deng. Lagconv: Local-context adaptive convolution kernels with global harmonic bias for pansharpening. In *Proceedings of the AAAI Conference on Artificial Intelligence*, volume 36, pages 1113–1121, 2022.

[Kingma and Ba, 2014] Diederik P Kingma and Jimmy Ba. Adam: A method for stochastic optimization. *arXiv preprint arXiv:1412.6980*, 2014.

[Kudo and Aoki, 2017] Yasunori Kudo and Yoshimitsu Aoki. Dilated convolutions for image classification and object localization. In *2017 Fifteenth IAPR international conference on machine vision applications (MVA)*, pages 452–455. IEEE, 2017.

[Li *et al.*, 2021] Duo Li, Jie Hu, Changhu Wang, Xiangtai Li, Qi She, Lei Zhu, Tong Zhang, and Qifeng Chen. Involution: Inverting the inherence of convolution for visual recognition. In *Proceedings of the IEEE/CVF Conference on Computer Vision and Pattern Recognition*, pages 12321–12330, 2021.

[Masi *et al.*, 2016] Giuseppe Masi, Davide Cozzolino, Luisa Verdoliva, and Giuseppe Scarpa. Pansharpening by convolutional neural networks. *Remote Sensing*, 8(7):594, 2016.

[Pan *et al.*, 2022] Xuran Pan, Chunjiang Ge, Rui Lu, Shiji Song, Guanfu Chen, Zeyi Huang, and Gao Huang. On the integration of self-attention and convolution. In *Proceedings of the IEEE/CVF conference on computer vision and pattern recognition*, pages 815–825, 2022.

[Paszke *et al.*, 2019] Adam Paszke, Sam Gross, Francisco Massa, Adam Lerer, James Bradbury, Gregory Chanan, Trevor Killeen, Zeming Lin, Natalia Gimelshein, Luca Antiga, et al. Pytorch: An imperative style, high-performance deep learning library. *Advances in neural information processing systems*, 32, 2019.

[Peng *et al.*, 2017] Chao Peng, Xiangyu Zhang, Gang Yu, Guiming Luo, and Jian Sun. Large kernel matters–improve semantic segmentation by global convolutional network. In *Proceedings of the IEEE conference on computer vision and pattern recognition*, pages 4353–4361, 2017.

[Qu *et al.*, 2017] Ying Qu, Hairong Qi, Bulent Ayhan, Chiman Kwan, and Richard Kidd. Does multispectral/hyperspectral pansharpening improve the performance of anomaly detection? In *2017 IEEE International Geoscience and Remote Sensing Symposium (IGARSS)*, pages 6130–6133. IEEE, 2017.

[Sandler *et al.*, 2018] Mark Sandler, Andrew Howard, Menglong Zhu, Andrey Zhmoginov, and Liang-Chieh Chen. Mobilenetv2: Inverted residuals and linear bottlenecks. In *Proceedings of the IEEE conference on computer vision and pattern recognition*, pages 4510–4520, 2018.

[Scarpa *et al.*, 2018] Giuseppe Scarpa, Sergio Vitale, and Davide Cozzolino. Target-adaptive cnn-based pansharpening. *IEEE Transactions on Geoscience and Remote Sensing*, 56(9):5443–5457, 2018.

[Su *et al.*, 2019] Hang Su, Varun Jampani, Deqing Sun, Orazio Gallo, Erik Learned-Miller, and Jan Kautz. Pixel-adaptive convolutional neural networks. In *Proceedings of the IEEE/CVF Conference on Computer Vision and Pattern Recognition*, pages 11166–11175, 2019.

[Szegedy *et al.*, 2016] Christian Szegedy, Vincent Vanhoucke, Sergey Ioffe, Jon Shlens, and Zbigniew Wojna. Rethinking the inception architecture for computer vision. In *Proceedings of the IEEE conference on computer vision and pattern recognition*, pages 2818–2826, 2016.

[Vaswani *et al.*, 2017] Ashish Vaswani, Noam Shazeer, Niki Parmar, Jakob Uszkoreit, Llion Jones, Aidan N Gomez, Łukasz Kaiser, and Illia Polosukhin. Attention is all you need. *Advances in neural information processing systems*, 30, 2017.

[Vivone *et al.*, 2020] Gemine Vivone, Mauro Dalla Mura, Andrea Garzelli, Rocco Restaino, Giuseppe Scarpa, Magnus O Ulfarsson, Luciano Alparone, and Jocelyn Chanussot. A new benchmark based on recent advances in multispectral pansharpening: Revisiting pansharpening with classical and emerging pansharpening methods. *IEEE Geoscience and Remote Sensing Magazine*, 9(1):53–81, 2020.

[Wu *et al.*, 2021a] Xiao Wu, Ting-Zhu Huang, Liang-Jian Deng, and Tian-Jing Zhang. Dynamic cross feature fusion for remote sensing pansharpening. In *Proceedings of the IEEE/CVF International Conference on Computer Vision*, pages 14687–14696, 2021.

[Wu *et al.*, 2021b] Xiao Wu, Ting-Zhu Huang, Liang-Jian Deng, and Tian-Jing Zhang. Dynamic cross feature fusion for remote sensing pansharpening. In *Proceedings of the IEEE/CVF International Conference on Computer Vision (ICCV)*, pages 14687–14696, October 2021.

[Xiao Wu and Ran, 2022] Liang-Jian Deng Xiao Wu and Ran Ran. "pancollection" for remote sensing pansharpening, 2022.

[Yang *et al.*, 2017] Junfeng Yang, Xueyang Fu, Yuwen Hu, Yue Huang, Xinghao Ding, and John Paisley. Pannet: A deep network architecture for pan-sharpening. In *Proceedings of the IEEE international conference on computer vision*, pages 5449–5457, 2017.

[Zamora Esquivel *et al.*, 2019] Julio Zamora Esquivel, Adan Cruz Vargas, Paulo Lopez Meyer, and Omesh Tickoo. Adaptive convolutional kernels. In *Proceedings of the IEEE/CVF international conference on computer vision workshops*, pages 0–0, 2019.

[Zhao *et al.*, 2023] Chen-Yu Zhao, Tian-Jing Zhang, Ran Ran, Zhi-Xuan Chen, and Liang-Jian Deng. Lgp-conv: learnable gaussian perturbation convolution for lightweight pansharpening. In *Proceedings of the Thirty-Second International Joint Conference on Artificial Intelligence*, pages 4647–4655, 2023.

[Zhou *et al.*, 2021] Jingkai Zhou, Varun Jampani, Zhixiong Pi, Qiong Liu, and Ming-Hsuan Yang. Decoupled dynamic filter networks. In *Proceedings of the IEEE/CVF Conference on Computer Vision and Pattern Recognition*, pages 6647–6656, 2021.